JGP Journal of General Physiology

ARTICLE

Engineered high-affinity zinc binding site reveals gating configurations of a human proton channel

Vladimir V. Cherny[1], Boris Musset[2], Deri Morgan[1], Sarah Thomas[3], Susan M.E. Smith[3], and Thomas E. DeCoursey[1]

The voltage-gated proton channel (H_V1) is a voltage sensor that also conducts protons. The singular ability of protons to penetrate proteins complicates distinguishing closed and open channels. When we replaced valine with histidine at position 116 in the external vestibule of hH_V1, current was potently inhibited by externally applied Zn^{2+} in a construct lacking the two His that bind Zn^{2+} in WT channels. High-affinity binding with profound effects at 10 nM Zn^{2+} at pH_o 7 suggests additional groups contribute. We hypothesized that Asp^{185}, which faces position 116 in our closed-state model, contributes to Zn^{2+} chelation. Confirming this prediction, V116H/D185N abolished Zn^{2+} binding. Studied in a C-terminal truncated monomeric construct, V116H channels activated rapidly. Anomalously, Zn^{2+} slowed activation, producing a time constant independent of both voltage and Zn^{2+} concentration. We hypothesized that slow turn-on of H^+ current in the presence of Zn^{2+} reflects the rate of Zn^{2+} unbinding from the channel, analogous to drug-receptor dissociation reactions. This behavior in turn suggests that the affinity for Zn^{2+} is greater in the closed state of hH_V1. Supporting this hypothesis, pulse pairs revealed a rapid component of activation whose amplitude decreased after longer intervals at negative voltages as closed channels bound Zn^{2+}. The lower affinity of Zn^{2+} in open channels is consistent with the idea that structural rearrangements within the transmembrane region bring Arg^{205} near position 116, electrostatically expelling Zn^{2+}. This phenomenon provides direct evidence that Asp^{185} opposes position 116 in closed channels and that Arg^{205} moves between them when the channel opens.

Introduction

Voltage-gated proton channels (H_V1s) are widely distributed both phylogenetically and among different human cells (DeCoursey, 2013). An overview of the human H_V1 (hH_V1) dimer is shown in Fig. 1. The gating of H_V1 remains a highly controversial and mysterious process. Largely by analogy with the voltage-sensing domain (VSD) of other voltage-gated ion channels, the S4 helix in H_V1 has been presumed to move outward during channel opening. This historical bias persists, despite the fact that in contrast with other channels in which VSD movement must pull open a physically distant pore formed by the S5-S6 helices, in H_V1 the conduction pathway resides within the VSD, thereby obviating any a priori need for a large conformational change (DeCoursey, 2015b). The extent of S4 movement in H_V1 has been modeled as one (Kulleperuma et al., 2013; Li et al., 2015; van Keulen et al., 2017) to three "clicks" or helical turns (Ramsey et al., 2010; Randolph et al., 2016), as well as intermediate values (Wood et al., 2012; Chamberlin et al., 2015; Gianti et al., 2016). The strongest type of evidence that S4 actually moves comes from differences in accessibility of specific sites in closed and open channels. Studies introducing Cys into S4 and probing with MTS reagents (Gonzalez et al., 2010) or introducing His into S4 and probing with Zn^{2+} (Kulleperuma et al., 2013; Morgan et al., 2013) appear to indicate that S4 moves outward at least one click. This class of evidence has been questioned because of the different side-chain volumes occupied by introduced amino acids (Kariev and Green, 2018). In addition, mutations neutralizing charged residues in S4 appear to alter gating movements (Gonzalez et al., 2013). Given these considerations, it would be useful to evaluate gating using probes directed toward other less mobile parts of the channel molecule. We were especially interested in identifying positions at which an engineered metal-binding site was differentially accessible to metals in closed and open channels. The approach of introducing metal-binding sites to assess state-dependent binding has been used successfully in other voltage-gated ion channels (Webster et al., 2004; Lee and MacKinnon, 2019). In this effort, we discovered a location where introduction of a single His produced extraordinary sensitivity of the channel to Zn^{2+}.

Externally applied Zn^{2+} inhibits WT proton currents potently (Thomas and Meech, 1982; Mahaut-Smith, 1989b; Eder et al.,

[1]Department of Physiology & Biophysics, Rush University, Chicago IL; [2]Institut für Physiologie und Pathophysiologie, Paracelsus Medizinische Privatuniversität, Nürnberg, Germany; [3]Department of Molecular and Cellular Biology, Kennesaw State University, Kennesaw, GA.

Correspondence to Thomas E. DeCoursey: tdecours@rush.edu; D. Morgan's present address is University of Kansas Medical Center, Kansas City, MO.

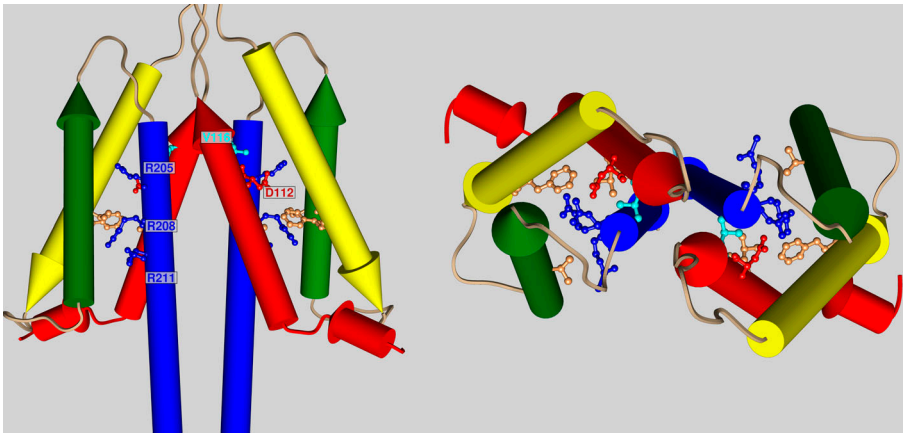

Figure 1. **Location of key amino acids in an hH_V1 dimer model.** Homology model of the closed hH_V1 dimer (Li et al., 2015) is shown in side view (left) and top view (right), where top corresponds to the extracytoplasmic side. Transmembrane helices are shown as pipes; connecting loops are shown as ribbons. The S1, S2, S3, and S4 helices are indicated in red, yellow, green, and blue, respectively. The hydrophobic gasket residues V109 (on S1), F150 (on S2), and V177 and V178 (on S3) are indicated in brown ball-and-sticks. Note that for clarity the side view is truncated above the strongest coiled-coil interaction of the C termini of the protomers.

1995; DeCoursey, 2003), with pronounced effects in mammalian cells at external pH, pH_o 7 occurring at 1 µM or higher (Schrenzel et al., 1996; Cherny and DeCoursey, 1999; Lishko et al., 2010). In addition to decreasing the maximum proton conductance (g_H), divalent metal cations prominently shift the g_H-V relationship of native proton currents positively and slow activation (Barish and Baud, 1984; Byerly et al., 1984; Cherny and DeCoursey, 1999; Chaves et al., 2020). Both of these effects are strongly inhibited at low pH_o, and quantitative modeling of the competition between Zn^{2+} and H^+ suggested that each Zn^{2+} ion binds to a site composed of at least two titratable groups with pK_a 6.5–7.0, most likely His (pK_a is the pH at which half the groups are protonated; Cherny and DeCoursey, 1999). This prediction was confirmed when the *HVCN1* gene was identified and found to contain two externally accessible His (His^{140} and His^{193}); most of the inhibition of H_V1 by Zn^{2+} is eliminated by mutating two Zn^{2+}-binding His in the H140A/H193A double mutant (Ramsey et al., 2006). The crystal structure of the mouse proton channel, mH_V1, contained a Zn^{2+} atom near His^{136} (His^{140} in hH_V1) and was consistent with its interaction also with His^{189} (His^{193} in hH_V1), which was, however, disordered and not resolved (Takeshita et al., 2014).

Here, we show that the effects of Zn^{2+} on V116H mutants were strikingly different from those on WT channels. We introduced this mutation into a background (H140A/H193A) in which we replaced the two His that comprise the main binding site for Zn^{2+} in WT channels (Ramsey et al., 2006; Musset et al., 2010b; Takeshita et al., 2014). A single His introduced at position 116 in the outer vestibule bound Zn^{2+} with an affinity many orders of magnitude greater than His in bulk solution or than the background construct (H140A/H193A). The extremely high affinity suggests that other groups contribute to Zn^{2+} binding. We identify Asp^{185} as providing an essential group.

The WT H_V1 channel in humans and many other species exists as a dimer in the plasma membrane (Koch et al., 2008; Lee et al., 2008; Tombola et al., 2008), illustrated in Fig. 1. Several lines of evidence indicate that interactions between the two protomers in the dimer during channel opening produce cooperative gating (Gonzalez et al., 2010; Musset et al., 2010b; Tombola et al., 2010). In some studies, we also removed the C terminus (H140A/H193A/T222stop) to preclude the possibility of interactions between protomers during gating. Serendipitously, because monomeric H_V1 opens much faster than the WT dimeric form, introducing V116H into this background revealed two components of apparent activation. Analysis of the kinetics indicated that Zn^{2+} binds mainly to closed channels and is expelled from the channel when it opens. This behavior provides clues to the closed and open structures and constrains the opening mechanism of hH_V1.

Materials and methods

Gene expression

Site-directed mutants were created using the Stratagene QuikChange (Agilent) procedure according to the manufacturer's instructions. Transfection into HEK-293 cells was done as described (Kulleperuma et al., 2013). No other voltage- or time-dependent conductances were observed under the conditions of this study. The level of expression of the mutants studied here was sufficiently high that contamination by native H_V1 was negligible.

Electrophysiology

In most experiments, cells expressing GFP-tagged proton channels were identified using Nikon inverted microscopes with fluorescence capability. For constructs that lacked the GFP tag, GFP was cotransfected. Conventional patch-clamp techniques were used (Kulleperuma et al., 2013) at room temperature (20–26°C). Bath and pipette solutions contained 60–100 mM buffer, 1–2 mM $CaCl_2$ or $MgCl_2$ (intracellular solutions were Ca^{2+}-free), 1–2 mM EGTA, and $TMAMeSO_3$ to adjust the osmolality to ∼300 mOsm, titrated with tetramethylammonium hydroxide (TMAOH). Buffers used were Homopipes at pH 5.0, Mes at pH 5.5–6.0, BisTris at pH 6.5, and PIPES at pH 7.0. Currents are shown without leak correction. To minimize changes in intracellular pH (pH_i) due to large H^+ fluxes, pulses for large depolarizations in pulse families were sometimes shortened.

We calculated free Zn^{2+} concentrations, $[Zn^{2+}]$, using WEBMAXC STANDARD from the MaxChelator series (Bers, 2009). This venerable program is currently based in the University of California at Davis, Davis, CA. We appreciate the help of Donald M. Bers, Eleonora Grandi, Brittany C. Kolb, and Daniel Cotton in facilitating access. The program includes metal and proton binding to buffers as a function of temperature and ionic strength.

Proton current amplitude (I_H) was usually determined by fitting the rising current with a single exponential and extrapolating to infinite time. g_H was calculated from I_H, and the reversal potential, V_{rev}, was measured in each solution: $g_H = I_H/(V - V_{rev})$. V_{rev} was determined by two methods, depending on the relative positions of V_{rev} and the threshold voltage for activation of the g_H, $V_{threshold}$. For constructs in which $V_{threshold}$ was positive to V_{rev}, the latter was determined by examining tail currents. Because hH_V1 currents were the only time-dependent conductance present, V_{rev} was established by the amplitude and direction of current decay during deactivation. By using this procedure, a time-independent leak or other extraneous conductances do not affect V_{rev}. Tail currents were not observed in nontransfected cells. For mutants in which $V_{threshold}$ was negative to V_{rev}, it was possible to observe directly the reversal of currents activated during pulse families.

Results

Part I: Experiments on dimeric channels

V116H mutant is potently inhibited by Zn^{2+}

To observe in isolation the effects of Zn^{2+} binding to a His introduced at position 116 (V116H), we first eliminated the two His that bind Zn^{2+} in WT hH_V1 (Ramsey et al., 2006). Fig. 2 A shows that this Zn^{2+}-insensitive construct (H140A/H193A) is only weakly inhibited by 100 µM Zn^{2+}, with more significant inhibition at 1 mM. Consequently, the effects of Zn^{2+} described below at lower concentrations are due almost entirely to the presence of His at position 116. The kinetics of activation is not noticeably affected by removal of these two His (Fig. 3). The most obvious effects of Zn^{2+} on the Zn^{2+}-insensitive background construct are decreased current amplitude and a positively shifted g_H-V relationship, with little change in kinetics. In this Zn^{2+}-insensitive background, introducing a single His at position 116 in the outer vestibule (V116H) increased the Zn^{2+} affinity drastically. Fig. 2 B shows that 10 nM Zn^{2+} profoundly inhibited H^+ currents at pH_o 7. The current amplitude was reduced, activation kinetics was slowed, and the g_H-V relationship was shifted positively, with larger effects on all three parameters at 100 nM Zn^{2+}. Qualitatively, these effects recapitulate the manifestations of Zn^{2+} inhibition of H_V1 in most mammalian cells (Cherny and DeCoursey, 1999), although the reduction of current amplitude appeared much more prominent than is observed in WT H_V1 channels. The affinity of this engineered Zn^{2+} binding site was so high that simply adding EGTA to nominally Zn^{2+}-free solutions relieved inhibition by unknown contaminants, presumably polyvalent metal cations. High-affinity Zn^{2+} binding sites exist in NMDA receptors, where a similar problem of heavy metal contamination of standard solutions was encountered (Paoletti et al., 1997). To establish a defined low concentration of free Zn^{2+}, $[Zn^{2+}]$, the solutions in Fig. 2 B were buffered with ADA (*N*-(2-Acetamido)iminodiacetic acid, *N*-(carbamoylmethyl)iminodiacetic acid), with $[Zn^{2+}]$ calculated using WEBMAXC STANDARD from the MaxChelator series (Materials and methods).

Fig. 4 illustrates that the single added His in V116H increased Zn^{2+} sensitivity, assessed by the reduction of current at +60 mV,

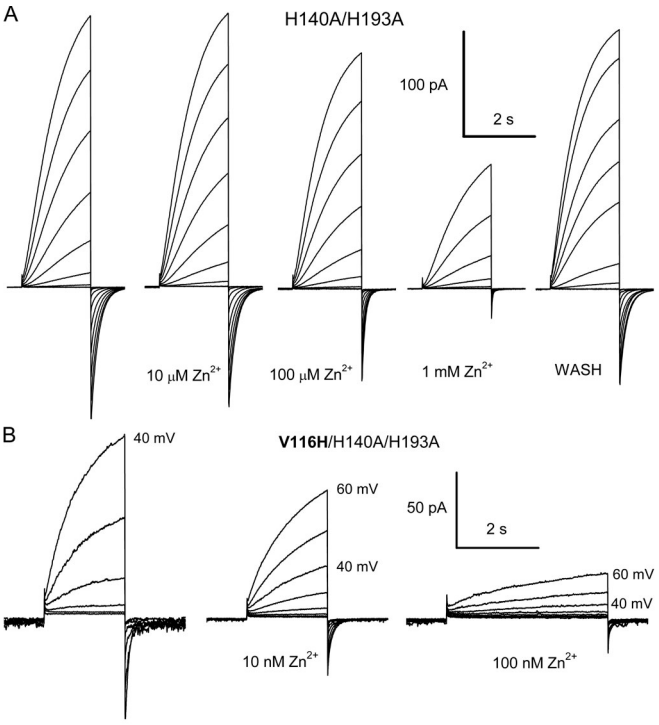

Figure 2. **Zn^{2+} binds very weakly to hH_V1 with His^{140} and His^{193} removed, but with extraordinarily high affinity when His is introduced at position 116 (V116H). (A)** The H140A/H193A background for dimer studies lacks the two His critical for Zn^{2+} binding and is insensitive to Zn^{2+} up to 100 µM. Families of currents in 10-mV increments up to +40 mV are shown for the indicated concentrations of Zn^{2+}, all at pH_o 7, pH_i 6.5. **(B)** Extreme Zn^{2+} sensitivity of V116H mutant in the H140A/H193A background. Families of currents at pH_o 7, pH_i 7 showing that 10 nM Zn^{2+} produces distinct inhibition. It is evident that in addition, τ_{act} is slowed and the g_H-V relationship is shifted positively.

by 5–6 orders of magnitude compared with the background double His mutant H140A/H193A. In fact, V116H is >100-fold more sensitive to Zn^{2+} than is WT hH_V1. To avoid the necessity of using buffered solutions for low Zn^{2+} concentrations, in many experiments we lowered the Zn^{2+} affinity by using pH_o 6 solutions. The V116H mutant was distinctly less sensitive to Zn^{2+} at pH_o 6 (Fig. 4, open symbols and dashed lines) than at pH_o 7, as was WT hH_V1. The inhibition of rat proton currents by Zn^{2+} was found previously to be extremely sensitive to pH_o, with lower affinity at lower pH_o, which was explained by Zn^{2+} competing with H^+ for two or more titratable groups (Cherny and DeCoursey, 1999).

Location of Val^{116} in closed and open hH_V1: What helps V116H bind Zn^{2+}?

The affinity of Zn^{2+} for His in solution is rather weak, K_d at pH 7.4, 25°C, and 0.1 M ionic strength is 322 µM (Krężel and Maret, 2016). The extraordinarily high affinity of Zn^{2+} for V116H strongly suggests that additional coordinating groups exist near this location and that steric factors are favorable. Examination of a closed state model of hH_V1 (Li et al., 2015) reveals that Asp^{185} is directly across the pore from position 116 (Fig. 5 A). To test whether Asp^{185} indeed contributes to the coordination of Zn^{2+},

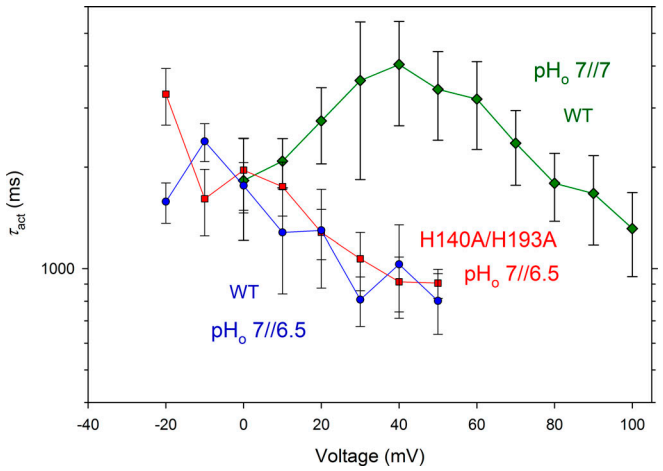

Figure 3. **The kinetics of activation is not changed in the Zn^{2+}-insensitive H140A/H193A mutant.** Turn-on of current was fitted with a single exponential. Direct comparison at pH_o 7 and pH_i 6.5 is shown, along with pH 7//7 WT data (from Cherny et al., 2015) for reference. Mean ± SEM is plotted for numbers of cells from negative to positive voltages: WT 5, 10, 12, 11, 11, 9, 10, and 3; and H140A/H193A 4, 6, 9, 9, 9, 6, 6, and 4. Although the values at −20 mV are just "significantly" different at P = 0.026, this is obviously a statistical aberration.

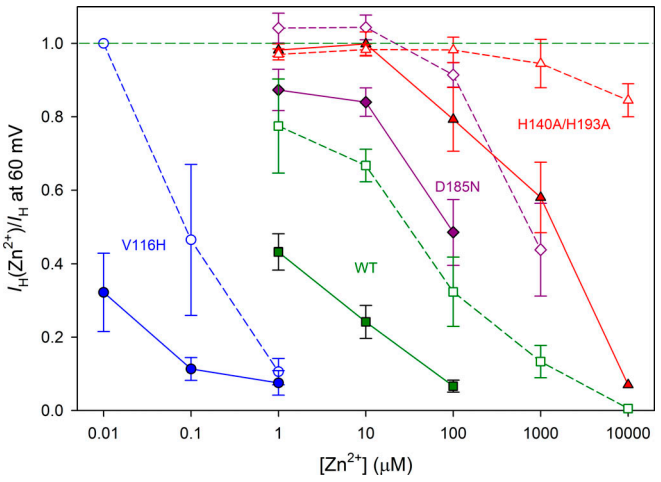

Figure 4. **Comparison of Zn^{2+} inhibition of proton current in V116H, D185N, and WT hH_V1 and in the Zn^{2+}-insensitive H140A/H193A background.** Inhibition of H^+ current by Zn^{2+} at +60 mV in the V116H/H140A/H193A mutant (●), WT hH_V1 (■), V116H/H140A/D185N/H193A (♦), and background construct H140A/H193A (▲). The mean ± SEM ratio of test pulse current in the presence of Zn^{2+} to its absence is plotted. Solid symbols and lines show measurements at pH_o 7, open symbols and dashed lines at pH_o 6. For concentrations <1 μM, Zn^{2+} was buffered with ADA. Numbers of cells, from low to high [Zn^{2+}], for V116H are 6, 3, and 6 at pH_o 7; 3, 3, and 8 at pH_o 6; for WT 13, 10 and 7 at pH_o 7; 4, 6, 5, 4, and 1 at pH_o 6; for V116H/D185N 3, 4, and 4 at pH_o 7; 4, 4, 4, and 3 at pH_o 6; and for H140A/H193A 2, 5, 6, 4, and 1 at pH_o 7; 3, 3, 3, 3, and 3 at pH_o 6.

we replaced this Asp with Asn, which is similar in size but lacks a negative charge. The V116H/H140A/D185N/H193A mutant (D185N) generated robust currents (Fig. 6) that were only weakly sensitive to Zn^{2+} either at pH_o 7 (Fig. 6, A–C) or at pH_o 6 (Fig. 6, D–F). Zn^{2+} begins to inhibit proton currents in this construct only at 100 μM at pH_o 7 and at 1 mM at pH_o 6 (Fig. 6 C and Fig. 4 F, respectively). The inhibition by Zn^{2+} is compared with WT and the Zn^{2+}-insensitive background construct (H140A/H193A) in Fig. 4. Combined with D185N, V116H may exhibit some anemic residual Zn^{2+} binding capability because it appears slightly more sensitive than the background construct. Nevertheless, it is evident that the potent Zn^{2+}-binding capability of His^{116} strictly requires Asp^{185} to facilitate coordination.

Part II: Experiments on monomeric channels

The WT hH_V1 channel exists as a dimer (Koch et al., 2008; Lee et al., 2008; Tombola et al., 2008), and interactions between the two protomers are thought to produce cooperative gating during channel opening (Gonzalez et al., 2010; Musset et al., 2010b; Tombola et al., 2010). To preclude complications resulting from inter-protomer interactions, we removed the C terminus as well as the two Zn^{2+}-binding His (H140A/H193A/T222stop) to produce mainly monomeric channels (Koch et al., 2008; Tombola et al., 2008; Musset et al., 2010b; Fujiwara et al., 2013). The Zn^{2+} sensitivity of this background construct (Fig. 7) was similar to that of the dimeric double mutant (H140A/H193A; Fig. 2 A); it was insensitive to 10 μM Zn^{2+}, with higher concentrations decreasing the current and shifting the g_H-V relationship positively, but with little effect on kinetics.

Next, we introduced His at position 116. Mammalian proton currents have notoriously slow opening kinetics, with activation time constants (τ_{act}) of 1–10 s at room temperature. Monomeric constructs have activation kinetics 3–17 times more rapid than the WT dimer (Koch et al., 2008; Tombola et al., 2008; Musset et al., 2010b; Fujiwara et al., 2013). Accordingly, the monomeric construct activated rapidly (Fig. 8, red symbols), as is evident by inspection of Fig. 2 A and Fig. 7. The V116H mutation itself apparently accelerated channel opening in the dimeric construct (Fig. 8, blue symbols). Much of this speeding is due to the lower pH_i 6 in these studies, however. The single mutant V116H in WT background (all His intact) at pH_o 7, pH_i 7 is only twice faster (Fig. 8, purple hexagons). Activation was not only rapid, but it also exhibited very little voltage dependence in the monomer. Kinetics was somewhat faster at pH_o 7 than 6, consistent with typical WT hH_V1 behavior.

Although the V116H mutation and monomerization of H_V1 both speed activation, it is unlikely that the V116H mutation itself produces monomerization. The dimer is stabilized by coiled-coil interactions at the C terminus (Koch et al., 2008; Lee et al., 2008; Tombola et al., 2008; Fujiwara et al., 2012, 2014), which remains intact. Position 116 faces the aqueous vestibule (Fig. 1 and Fig. 5) and is not well positioned to participate in any proposed dimer interface (Lee et al., 2008; Musset et al., 2010a, 2010b; Takeshita et al., 2014). Finally, H_V1 may differ from other voltage-gated ion channels by virtue of the observation that gating kinetics was altered by nearly all point mutations in which it was studied (DeCoursey et al., 2016).

Zn^{2+} has qualitatively different effects on the V116H monomer than on WT channels

Families of currents generated by the V116H monomer (V116H/H140A/H193A/T222stop) are shown in Fig. 9. Row A is at pH_o 6,

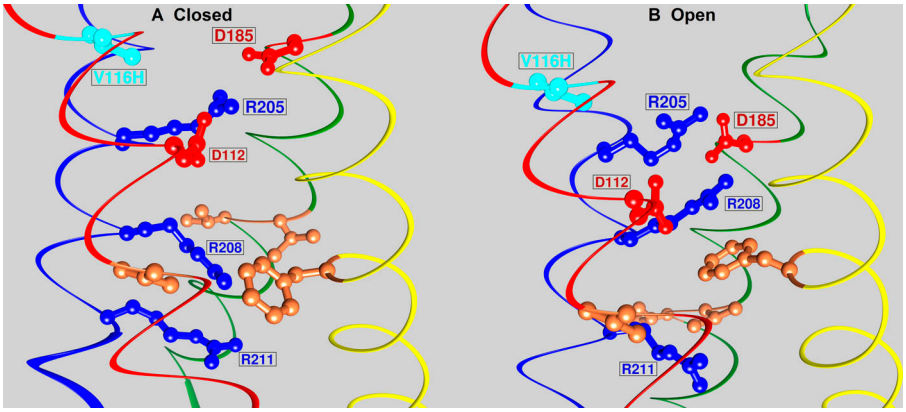

Figure 5. **Map of key amino acids in closed and open hH_V1 models. (A and B)** Alpha carbons of S2 helices (yellow ribbon) of closed (A, left) and open (B, right) homology models of human H_V1 (Li et al., 2015) were superimposed using the Matchmaker program in Chimera (resource for Biocomputing, Visualization, and Informatics, University of California, San Francisco, San Francisco, CA; supported by NIGMS P41-GM103311; Pettersen et al., 2004) and are shown at the same viewing angle. S1, S2, S3, and S4 helices are indicated as red, yellow, green, and blue ribbons, respectively. The hydrophobic gasket residues V109 (on S1), F150 (on S2), and V177 and V178 (on S3) are indicated in brown.

row B is at pH_o 7, and in both the effects of Zn^{2+} are profound. Drastic effects are already apparent at 1 µM Zn^{2+}: decreased current amplitude, a massive slowing of apparent activation, and a positive shift of the g_H-V relationship indicated by activation occurring at higher voltages. Surprisingly, however, the currents at 10 µM or 100 µM Zn^{2+} appear kinetically similar to those at 1 µM Zn^{2+} and seem to differ mainly in their g_H-V relationships being shifted more positively. In WT proton channels, Zn^{2+} and other divalent metal cations slow activation profoundly, but this effect increases distinctly with higher concentrations (Barish and Baud, 1984; Byerly et al., 1984; Mahaut-Smith, 1989a; Kapus et al., 1993; Cherny and DeCoursey, 1999; Musset et al., 2010b; Chaves et al., 2020). The slowing of activation by divalent metal cations in WT channels is greater than can be accounted for by the positive shift of the g_H-V relationship (Byerly et al., 1984; Kapus et al., 1993; Cherny and DeCoursey, 1999; Chaves et al., 2020). The phenomenology of Zn^{2+} interaction with the V116H monomer thus differs drastically from Zn^{2+} effects on WT channels. Fig. 9, C and D shows that the activation of this construct is quite rapid (τ_{act} ranges from 200 to 300 ms at both pH_o 6 and pH_o 7) and is nearly independent of voltage. In WT H_V1 channels, τ_{act} becomes distinctly faster at higher voltages, both in the absence or presence of Zn^{2+} or other divalent metals (Barish and Baud, 1984; Byerly et al., 1984; Mahaut-Smith, 1989a; Kapus et al., 1993; Cherny and DeCoursey, 1999; Chaves et al., 2020). There is a suggestion in the V116H data that τ_{act} in the presence of Zn^{2+} actually slows at large positive voltages. Most surprisingly, the kinetics appears identical at all [Zn^{2+}]. In summary, in the V116H monomer, the activation kinetics in Zn^{2+} appears to be nearly independent of voltage, pH_o, and Zn^{2+} concentration.

The slowing of activation by divalent metals in WT H_V1 channels has been ascribed to the metals inhibiting channel opening (Cherny and DeCoursey, 1999; Qiu et al., 2016), and the

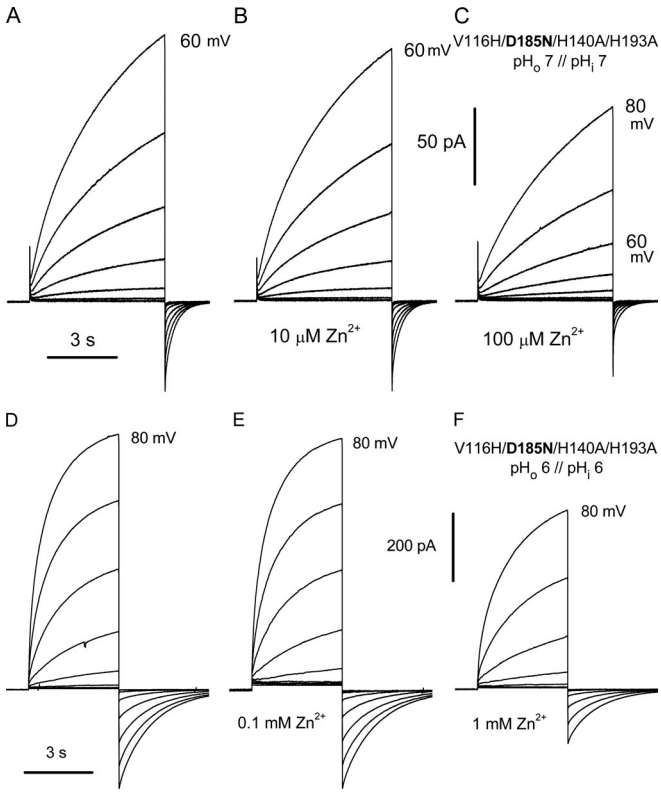

Figure 6. **Addition of the D185N mutation eliminates the Zn^{2+} sensitivity of V116H in the H140A/H193A background. (A–C)** A cell at pH_o 7, pH_i 7 is distinctly inhibited by 100 µM Zn^{2+}. Families were generated by pulses from V_{hold} = −40 mV in 10-mV increments from −10 mV up to the voltage indicated. **(D–F)** A different cell at pH_o 6, pH_i 6 is inhibited only at 1 mM Zn^{2+}. Families were generated by pulses from V_{hold} = −40 mV in 10-mV increments from 0 mV up to +80 mV.

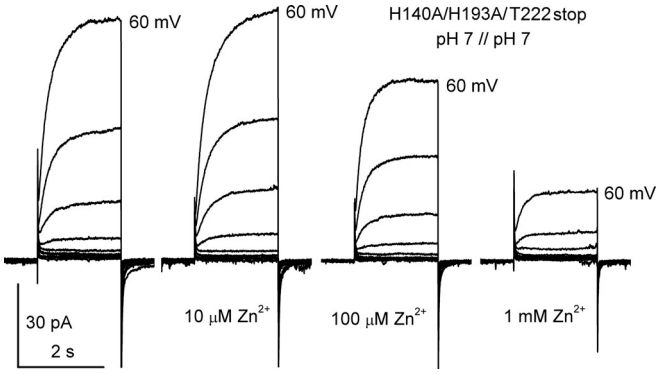

Figure 7. **The monomeric construct is insensitive to Zn^{2+}.** Zn^{2+} exerted minimal effects on the background construct used in this study, in which the two His that bind Zn^{2+} in WT channels were replaced with Ala, and the C terminus was truncated at position T222 (so that the final amino acid was K221).

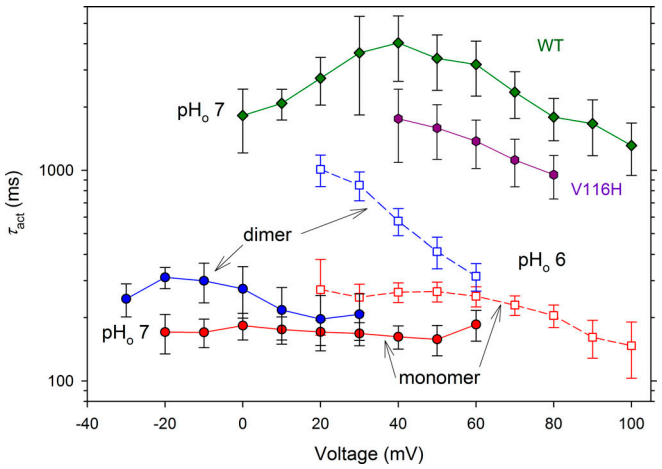

Figure 8. **Activation kinetics in the absence of Zn^{2+} in V116H/H140A/H193A constructs used here.** Values for τ_{act} (mean ± SEM) are plotted for dimeric (blue) and monomeric (red) V116H mutants at pH$_o$ 7 (solid symbols and lines) and pH$_o$ 6 (open symbols and dashed lines), all with pH$_i$ 6. For comparison, τ_{act} from WT hH$_V$1 is plotted (green) at pH$_o$ 7, pH$_i$ 7 (from Cherny et al., 2015), as well as the single mutant V116H at pH pH$_o$ 7 and pH$_i$ 7 (purple hexagons). It should be noted that τ_{act} with pH$_i$ 7 is substantially slower than with pH$_i$ 6. Numbers of cells starting at the most negative voltage are WT 3, 3, 6, 9, 11, 12, 12, 12, 12, 8, and 6; pH$_o$ 7 dimer 3, 4, 4, 4, 4, 4, and 3; pH$_o$ 6 dimer 4, 4, 4, 4, and 4; pH$_o$ 7 monomer 5, 8, 9, 10, 10, 10, 10, 7, and 3; and pH$_o$ 6 monomer 3, 3, 14, 15, 15, 15, 13, 4, and 3.

concentration-dependent effects on both kinetics and on the position of the g_H-V relationship can be described quantitatively by assuming the channel cannot open while bound by Zn^{2+} (Cherny and DeCoursey, 1999). The extraordinary concentration independence of Zn^{2+} effects on kinetics in the V116H monomer appears to indicate a different mechanism and is reminiscent of the concentration independence of the unbinding of drugs from their receptors. If the slow apparent activation in the presence of Zn^{2+} reflects the kinetics of Zn^{2+} unbinding from hH$_V$1, this implies that the affinity of the closed state is much higher than that of the open state. In other words, channel opening lowers the affinity of the channel for Zn^{2+}, resulting in its release. The following simple model describes this phenomenon (Scheme 1):

$$Closed \bullet Zn^{2+} \underset{on[Zn^{2+}]}{\overset{off}{\rightleftharpoons}} Closed \underset{\beta}{\overset{\alpha}{\rightleftharpoons}} Open$$

(Scheme 1)

From Fig. 9, C and D, it is evident that the unbinding rate ($off \approx 1/\tau_{act}$) for Zn^{2+} from closed channels is low (0.1–0.5 s^{-1}), whereas the opening rate ($\alpha \approx 1/\tau_{act}$) is faster by an order of magnitude or more. Consequently, the $Closed \bullet Zn^{2+} \rightarrow Open$ transition will be dominated by the unbinding rate (off). We therefore designed experiments to test whether Zn^{2+} binding to the V116H monomer is state dependent, as portrayed in Scheme 1.

It was sometimes possible to discern transitions between the three states of Scheme 1 at low Zn^{2+} concentrations. Fig. 10, A and B shows families of currents at 0.1 and 10 µM Zn^{2+}, respectively. At the lower concentration, there clearly are rapid as well as slow components of current increase during depolarizing pulses. At the higher concentration, the slow component dominates (as it does throughout Fig. 9). Superimposing the currents at +90 mV in this experiment (Fig. 10 C) shows that the rapid component disappears at higher Zn^{2+} concentrations. We interpret the rapid component as the "normal" opening process of closed channels that do not have Zn^{2+} bound to them. At higher [Zn^{2+}], essentially all (closed) channels have Zn^{2+} bound at the holding potential (V_{hold}) and thus only the slowly rising current reflecting unbinding kinetics is observed.

Zn^{2+} binding to V116H channels exhibits state dependence

Does τ_{act} actually reflect Zn^{2+} unbinding kinetics? We will assume that Zn^{2+} binds to the closed monomeric channel, where it either occludes the conduction pathway or prevents opening. In Fig. 11, A and B, we applied a depolarizing pulse to remove Zn^{2+} from many channels, with the rising current reflecting the appearance of channels that are Zn^{2+} free and open. The entire current during this first pulse rose slowly, indicating that before the pulse all channels were closed and Zn^{2+} bound. Then we repolarized for variable times during which the channels should close and gradually bind Zn^{2+} again due to its high affinity for closed channels. If we apply a second depolarizing pulse after a short interval, the current should reflect a mixture of (1) channels still open, (2) channels that have closed but are still free of Zn^{2+}, and (3) channels that have closed and rebound Zn^{2+}. The time course of channel closing is evident directly from the tail current upon repolarization. During the subsequent depolarization, still-open channels will give rise to an instantaneous jump in current. Channels that are closed but Zn^{2+} free should open at the rapid rate characteristic of V116H channels in the absence of Zn^{2+} (Fig. 9). Finally, those channels that closed and rebound Zn^{2+} during the interval should produce a slowly activating component as the opening process expels Zn^{2+} from the channel.

Fig. 11 shows experiments done to determine whether these three components exist and are occupied according to Scheme 1. In Fig. 11, A and B, a pair of pulses to +60 mV was applied with a variable interval between them. The current elicited by the first pulse rose slowly. In contrast, during the second pulse applied after a short interval, there was an instantaneous jump (channels still open), followed by a rapidly rising component ($Closed \rightarrow Open$), and finally a slowly rising phase ($Closed \bullet Zn^{2+} \rightarrow Open$). During the second pulse, channels that were still open remained open, producing an instantaneous jump on depolarization. Channels that closed but were not yet blocked by Zn^{2+} during the interval should open with the same rapid time course seen in the absence of Zn^{2+} (●; Fig. 9, C and D). As the tail current abates, the instantaneous jump decreases in amplitude, with a generally similar time course. In addition, the rapidly rising component becomes smaller as more channels become blocked ($Closed \rightarrow Closed \bullet Zn^{2+}$) at V_{hold}. The disappearance of the rapidly rising component should reflect the rate of Zn^{2+} binding to closed channels at V_{hold} (although they must close before becoming blocked). Channels that close and bind Zn^{2+} again should reopen with the slow time course that reflects Zn^{2+} unbinding

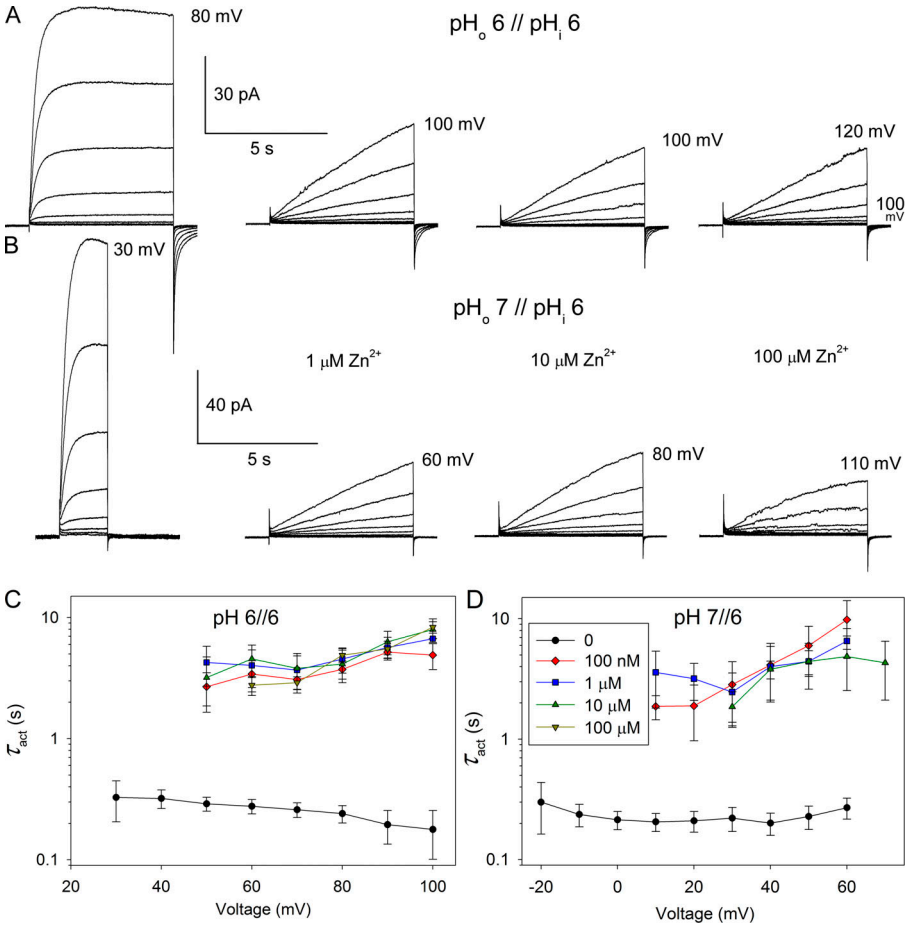

Figure 9. **In the V116H monomer, the turn-on of current in the presence of Zn^{2+} is practically independent of both voltage and Zn^{2+} concentration. (A and B)** Families of currents are shown at pH_o 6 (A) and pH_o 7 (B), both with pH_i 6, in the indicated concentrations of Zn^{2+} with pulses applied in 10-mV increments up to the voltage shown. **(C and D)** The τ_{act} values (mean ± SEM) from these cells are shown in the absence (●) or presence of Zn^{2+} in concentrations indicated in the inset to D. Every τ_{act} value at every voltage is significantly ($P < 0.05$) higher in Zn^{2+} than in control in C and D except two values at +60 mV in D. Numbers of cells at pH_o 6 are control 3–10, 100 nM Zn^{2+} 2–7, 1 μM Zn^{2+} 2–8, 10 μM Zn^{2+} 3–6, and 100 μM Zn^{2+} 3–5; numbers of cells at pH_o 7 are control 3–7, 100 nM Zn^{2+} 2 or 3, 1 μM Zn^{2+} 2–4, and 10 μM Zn^{2+} 3. The control values are a subset of those plotted in Fig. 8; here, we include only cells in which we also had τ_{act} data in Zn^{2+}.

kinetics. The three predicted components during the second pulse are all evident in Fig. 11. After a long interval at −60 mV, all the channels reopened with a slow time course, essentially identical to the current seen during the first pulse (Fig. 11 A). After short intervals, both an instantaneous jump and then an initial rapid rising phase can be seen.

If this interpretation is correct, one might predict that if the voltage during the interpulse interval differs from V_{hold}, the rate at which these transitions occur should change. In Fig. 11 B, we tested this by stepping to 0 mV during the interpulse interval. The tail current was now outward and decayed more slowly than it did at −60 mV in Fig. 11 A. The envelope of instantaneous current jumps during the depolarizing pulses was clearly slower than in Fig. 11 A. The presence of a distinct rapidly rising component also was visible after longer intervals than in Fig. 11 A.

Another prediction of Scheme 1 is that if the rapidly rising component reflects channels that were unblocked and opened by the preceding pulse, then if the first pulse is short, only a few channels will have had the opportunity to become unblocked. Therefore, as we lengthen the first pulse, more channels should open and become unblocked and the rapid component should increase in amplitude. Fig. 11 C illustrates this kind of experiment. The second pulse following a brief depolarization exhibited almost no fast component but had a larger instantaneous jump because repolarization was too brief for all the open channels to close. As the first pulse became longer, the rapidly

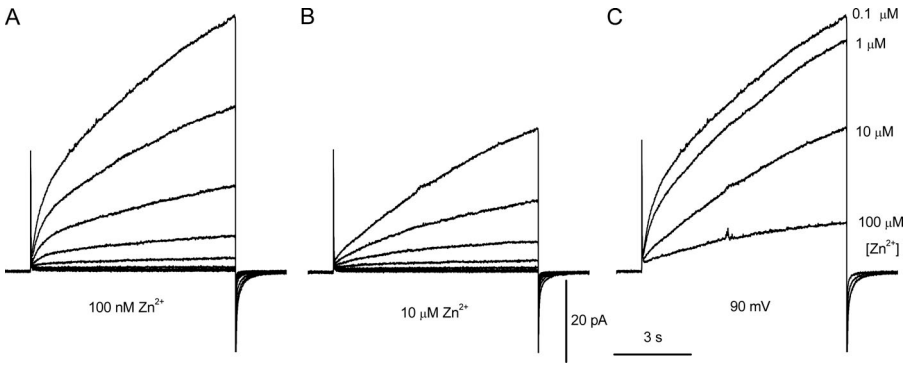

Figure 10. **Families of currents in the V116H monomer at pH 6//6. (A and B)** Pulses are in 10-mV increments from V_{hold} = −40 mV to +90 mV. Note that there is a distinct rapidly rising phase in A at 100 nM Zn^{2+} but not in B at 10 μM Zn^{2+}. **(C)** In the same cell, currents at +90 mV are superimposed in the presence of the indicated Zn^{2+}. The fast component is only detectable at low [Zn^{2+}].

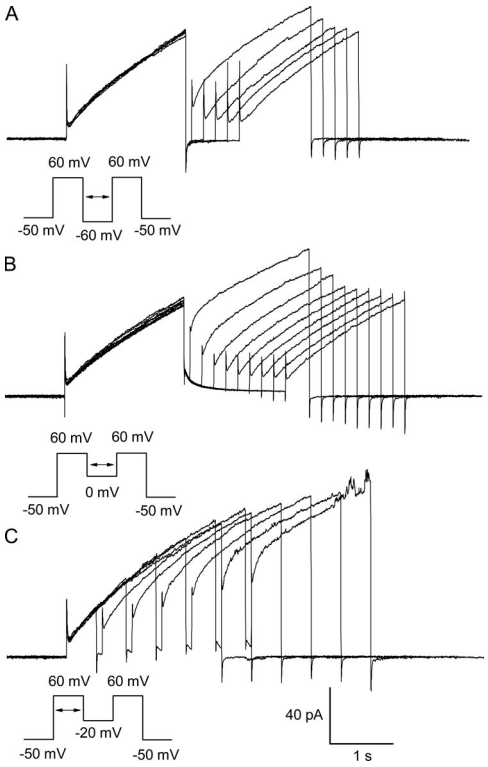

Figure 11. **Pulse pair experiments in the V116H monomer (V116H/H140A/H193A/T222stop) reveal two components of "activation." (A and B)** Panels differ only in the interpulse voltages of −60 mV or 0 mV, respectively. **(C)** The first pulse duration was varied. All measurements were from a cell at pH_o 7, pH_i 6 with 1 µM Zn^{2+}.

rising component increased in amplitude, as did the instantaneous jump. In all experiments in Fig. 11, fitting the current during the second pulse with two exponentials revealed that the two time constants remained constant, but their amplitudes varied. In a number of similar measurements, the fast and slow time constants extracted were variable but usually were reasonably close to τ_{act} in the absence of Zn^{2+} and τ_{act} in the presence of Zn^{2+}, respectively. For example, in the cell in Fig. 11, in the absence of Zn^{2+} at pH_o 7, τ_{act} was independent of voltage and averaged 236 ms, and the fast component τ_{act} in 1 µM Zn^{2+} in Fig. 11 B ranged from 78 to 317 ms. For the first pulse in Fig. 11 B, τ_{act} was 3.1 ± 0.71 s (n = 11), and the slower component in double exponential fits of the second pulse was 3.4 ± 0.36 s (n = 10; P = 0.24).

Discussion

The phenomenology of Zn^{2+} effects on V116H and WT H_V1 channels is strikingly different. In WT channels, it was possible to explain the slowing of activation and the shift of the g_H-V relationship by making a single assumption, that the channel cannot open with Zn^{2+} bound (Cherny and DeCoursey, 1999). The measured macroscopic rate of opening depends directly on the fraction of channels that have no Zn^{2+} bound. For example, at the K_d for Zn^{2+} binding, 50% of the channels are Zn^{2+} bound and τ_{act} is accordingly twice slower. If the opening rate is slowed but the closing rate is not affected, the g_H-V relationship shifts positively. These relationships do not hold for the V116H mutant. The decrease in current amplitude was much more pronounced than in WT hH_V1. The most remarkable phenomenon occurred in monomeric constructs. Because activation of monomeric H_V1 is much faster than of dimeric channels (Koch et al., 2008; Tombola et al., 2008; Musset et al., 2010b; Fujiwara et al., 2013), two components could be distinguished. At very low [Zn^{2+}], a rapid component with a time constant like that in the absence of Zn^{2+} was observed, together with a very slow component (τ was 2–10 s; Fig. 9). At 1 µM or higher [Zn^{2+}], the current generally turned on with a single slow time constant that was independent of both Zn^{2+} concentration and voltage. The simplest explanation is provided by analogy with drug–receptor interactions in which drug unbinding is independent of concentration. "Block" of V116H is purely state dependent, with extremely high-affinity binding to closed channels and essentially no affinity for open channels. In this view, Zn^{2+} affinity is so high that for 1 µM or higher [Zn^{2+}], essentially all channels in a closed state have Zn^{2+} attached. Zn^{2+} unbinding allows rearrangement of the protein that results in channel opening. The different phenomenology of WT and V116H channels evidently results mainly from the slow off rate for Zn^{2+} in V116H channels.

The combination of rapid activation kinetics of the monomeric construct combined with the slow off rate of Zn^{2+} made it possible to detect two clear components of turn-on of current in the presence of Zn^{2+}. Several kinds of data support the interpretation that the rapid opening in the presence of Zn^{2+} reflects normal opening kinetics of the mutant channels. The slower component appears to reflect the rate of Zn^{2+} unbinding as channels open. Like drug dissociation kinetics, Zn^{2+} dissociation occurs at the same rate independently of Zn^{2+} concentration. Fitting with two exponentials produces two time constants that are close to those of activation of the V116H channel in the absence of Zn^{2+} and the slow component that dominates at high Zn^{2+} concentrations. Varying pulse durations produce changes in the amplitudes of fast and slow components that are consistent with expectations of Scheme 1. The simple model in Scheme 1 can occur only if the affinity of the channel for Zn^{2+} is much lower when the channel opens. The present evidence strongly indicates that Zn^{2+} binds almost exclusively to closed V116H channels.

What explains the extraordinarily high affinity of Zn^{2+} binding to V116H?

The affinity of Zn^{2+} for His in solution is rather weak; K_d is 322 µM at pH 7.4, 25°C, and 0.1 M ionic strength (Krężel and Maret, 2016). Higher-affinity Zn^{2+} binding to catalytic sites in proteins typically results from tetrahedral coordination by liganding groups, usually His, Glu, Asp, or Cys and water (Alberts et al., 1998; Auld, 2001). The native Zn^{2+} binding site in hH_V1 and mH_V1 comprises two His (His^{140} and His^{193} in hH_V1; Ramsey et al., 2006; Musset et al., 2010b) with minor contributions from E119 and D123 (in mH_V1 with hH_V1 numbering; Takeshita et al., 2014). Some studies concluded that these residues produced two distinct metal binding sites in several species (Qiu et al., 2016; Chaves et al., 2020; Jardin et al., 2020). Although

native H_V1 channels from mammalian species are clearly inhibited by 1 or even 0.1 µM Zn^{2+} (Cherny and DeCoursey, 1999; Lishko et al., 2010), distinct effects on the single His at position 116 were observed at 10 nM Zn^{2+} (Fig. 2 B). Quantified by the decrease of current, Zn^{2+} is at least two orders of magnitude more potent for V116H than for WT channels (Fig. 4).

The potent Zn^{2+} binding suggests that other coordinating groups participate. Position 116 in the closed channel model of hH_V1 is reasonably near three acidic groups (D112, E119, and D185) that are potential candidates. Position 116 is between D112 and E119 vertically but is directly across from D185 (Fig. 5). The negativity of Asp^{185} would be expected to strongly enhance Zn^{2+} affinity (Gurd and Wilcox, 1956). To test whether Asp^{185} does indeed contribute, we replaced it with Asn, D185N. Fig. 6 shows that replacing Asp^{185} with Asn abolished high-affinity Zn^{2+} binding to His^{116}. We conclude from the high-affinity Zn^{2+} binding to His^{116} in the presence of Asp^{185} that these two positions are at a similar height in the closed channel.

State-dependent Zn^{2+} binding to His^{116} and Asp^{185} defines interactions in closed and open hH_V1 channels

Despite a crystal structure (Takeshita et al., 2014), electron paramagnetic resonance measurements (Li et al., 2015), and a profusion of homology models and MD simulations (Musset et al., 2010b; Ramsey et al., 2010; Wood et al., 2012; Kulleperuma et al., 2013; Morgan et al., 2013; Chamberlin et al., 2014, 2015; Pupo et al., 2014; Gianti et al., 2016; Qiu et al., 2016; Randolph et al., 2016; van Keulen et al., 2017; Banh et al., 2019; Jardin et al., 2020), there is little certainty with respect to closed or open structures or the molecular rearrangements that occur during gating. Depolarization of V116H presumably rearranges the channel protein, drastically lowering Zn^{2+} affinity. As Zn^{2+} unbinds, current appears. What drives Zn^{2+} unbinding? Is the binding site within the electric field? If this were the case, greater depolarization would remove Zn^{2+} faster and more completely. Contradicting this proposal, τ_{act} appears roughly independent of voltage in the presence of Zn^{2+} or perhaps even slows at increasingly positive voltages. However, because Zn^{2+} unbinding (*off*) is much slower than channel opening (α), any voltage dependence could be masked. We conclude that Zn^{2+} simply has a much lower affinity in the open state.

An explanation for state-dependent Zn^{2+} binding is suggested by comparing closed and open hH_V1 models based on electron paramagnetic resonance measurements of hH_V1 (Li et al., 2015) and informed by crystal structures of "down" and "up" (representing hyperpolarized and depolarized configurations, respectively) of the CiVSP (*Ciona intestinalis* voltage sensing phosphatase; Li et al., 2014). In the closed state, R1 (Arg^{205} in hH_V1) interacts with Asp^{112}, leaving sidechains at position 116 and Asp^{185} available for interaction. This interaction is supported by the crystal structure of closed mH_V1 (Takeshita et al., 2014). To reach the open state, the protein rearranges (DeCoursey, 2015a; Li et al., 2015) such that Asp^{112} can interact with Arg^{208} (Kulleperuma et al., 2013; Li et al., 2015), forming the selectivity filter (Musset et al., 2011). This rearrangement also inserts Arg^{205} directly between sidechains at position 116 and Asp^{185}. The intrusion of cationic Arg^{205} in the middle of the Zn^{2+}-binding site would repel Zn^{2+} electrostatically. This intuitive view suggests that as the channel begins its opening transition, as a result of the conformational change Arg^{205} repels the Zn^{2+}. Any voltage dependence that might be expected is overshadowed by the high affinity of binding, such that the slow off rate in Scheme 1 dominates.

MD simulations by Qiu et al. (2016) predict two Zn^{2+} binding sites in CiH_V1. The deeper site (from the outside) corresponding to Asp^{112} and Asp^{185} in hH_V1 was predicted to be more accessible to Zn^{2+} in the closed state. This is generally consistent with the experimental evidence presented here, and we demonstrate that, in all likelihood, in V116H Zn^{2+} is coordinated by the introduced His^{116} and by Asp^{185}. In the Li model of closed hH_V1, positions 116 and 185 are directly across the pore from each other (Li et al., 2015). In contrast, in the crystal structure of the closed mH_V1 (Takeshita et al., 2014), Asp^{185} is distinctly lower than position 116 (both human numbering). To date, no crystal structure exists of the entire H_V1 protein from any species, perhaps due to its high protein mobility (Li et al., 2015). The existing crystal structure is a chimera of mouse H_V1, with its N terminus truncated, its C terminus replaced by a leucine-zipper motif of the transcriptional activator GCN4 from *Saccharomyces cerevisiae*, and with a section of *C. intestinalis* voltage-sensing phosphatase spliced in from the middle of S2 to the middle of S3. It has been suggested that insertion of the CiVSP peptide at the inner side of S2-S3 resulted in S3 in the crystal structure being too low by one helical turn (DeCoursey, 2015a; Li et al., 2015; Banh et al., 2019). Thus, the high-affinity Zn^{2+} binding observed here between V116H and D185 supports the Li et al. closed state model.

In summary, the Zn^{2+} sensitivity of the V116H mutant strongly suggests that the closed model of hH_V1 proposed by Li et al. (2015) more closely reflects the closed channel structure than does the crystal structure of mH_V1 (Takeshita et al., 2014), specifically in the region including the inner ends of the S2 and S3 helices. In the closed state, position 116 is directly across the pore from Asp^{185}; and these two positions in the V116H mutant form an extremely high-affinity binding site for Zn^{2+}. These relationships exist in a closed state near the open state, but it is possible that deeper closed states exist. The most straightforward explanation for the loss of Zn^{2+} affinity in open channels is that repositioning of S4 brings Arg^{205} between His^{116} and Asp^{185}, expelling Zn^{2+} electrostatically. Our open state model requires no further movement of S4, but based on the present data, we cannot rule out the possibility that S4 might proceed farther. However, R211H mutants are inhibited by internally applied Zn^{2+}, supporting the idea that in the open state Asp^{112} interacts with Arg^{208} (Kulleperuma et al., 2013; Morgan et al., 2013). It is difficult to escape the conclusion that during opening, hH_V1 at a minimum traverses the two experimentally defined positions depicted in Fig. 5.

The relatively small excursion of S4 in closed and open states resolved here may appear to contradict the gating charge estimated for H_V1 by measurements of the limiting slope of the g_H-V relationship (Almers, 1978). For native (DeCoursey and Cherny, 1996, 1997) and WT dimeric channels (Musset et al., 2008; Fujiwara et al., 2012; Gonzalez et al., 2013; Thomas et al., 2018),

the gating charge tends toward the higher end of 4–6 e_0. For monomeric constructs, e_0 is half that (Gonzalez et al., 2010; Fujiwara et al., 2012; Gonzalez et al., 2013). If one assumes that the gating charge reflects the charge of all three Arg from S4 moving across the entire membrane electrical field, the smaller movement implied by the present results would appear to produce too little charge movement. However, charges in proteins other than Arg may contribute; for example, anionic charges on S1 may move inward (Mony et al., 2015). More importantly, gating current can result from obligatory protonation of internal acidic groups and deprotonation of external ones. This mechanism was proposed in a model that explained quantitatively the mechanism of ΔpH-dependent gating (Cherny et al., 1995), the establishment of the position of the g_H-V relationship by the pH gradient (ΔpH = pH_o − pH_i). An updated, but less quantitative version of this idea was proposed recently (the "counter-charge model") that emphasized the natural way in which the breaking and forming of salt bridges within the channel protein stabilizes closed and open states in a manner consistent with its producing ΔpH-dependent gating (DeCoursey, 2018). Protonation/deprotonation of sites within the membrane electrical field is practically indistinguishable from the gating charge resulting from the more traditional movement of charged groups within the protein.

Acknowledgments

Christopher J. Lingle served as editor.

This work was supported by National Institutes of Health grant R35 GM126902 (to T.E. DeCoursey), Deutsche Forschungsgemeinschaft grant MU 3574/4-1 (to B. Musset), and Bears Care (to D. Morgan). The content is solely the responsibility of the authors and does not necessarily represent the official views of the National Institutes of Health.

The authors declare no competing financial interests.

Author contributions: S.M.E. Smith and T.E. DeCoursey conceptualized the study. T.E. DeCoursey interpreted the data. V.V. Cherny, D. Morgan, B. Musset, and T.E. DeCoursey conducted experiments and performed the data analysis. T.E. DeCoursey, D. Morgan, and B. Musset acquired the funding. S.M.E. Smith and T.E. DeCoursey administered the project. S. Thomas and S.M.E. Smith provided resources. T.E. DeCoursey wrote the original draft of the manuscript. All authors reviewed and approved the manuscript.

Submitted: 19 May 2020
Accepted: 10 August 2020

References

Alberts, I.L., K. Nadassy, and S.J. Wodak. 1998. Analysis of zinc binding sites in protein crystal structures. *Protein Sci.* 7:1700–1716. https://doi.org/10.1002/pro.5560070805

Almers, W. 1978. Gating currents and charge movements in excitable membranes. *Rev. Physiol. Biochem. Pharmacol.* 82:96–190. https://doi.org/10.1007/BFb0030498

Auld, D.S. 2001. Zinc coordination sphere in biochemical zinc sites. *Biometals.* 14:271–313. https://doi.org/10.1023/A:1012976615056

Banh, R., V.V. Cherny, D. Morgan, B. Musset, S. Thomas, K. Kulleperuma, S.M.E. Smith, R. Pomès, and T.E. DeCoursey. 2019. Hydrophobic gasket mutation produces gating pore currents in closed human voltage-gated proton channels. *Proc. Natl. Acad. Sci. USA.* 116:18951–18961. https://doi.org/10.1073/pnas.1905462116

Barish, M.E., and C. Baud. 1984. A voltage-gated hydrogen ion current in the oocyte membrane of the axolotl, *Ambystoma*. *J. Physiol.* 352:243–263. https://doi.org/10.1113/jphysiol.1984.sp015289

Bers, D. 2009. WEBMAXC STANDARD. University of California, Davis. https://somapp.ucdmc.ucdavis.edu/pharmacology/bers/maxchelator/webmaxc/webmaxcS.htm (accessed June 2019)

Byerly, L., R. Meech, and W. Moody, Jr.. 1984. Rapidly activating hydrogen ion currents in perfused neurones of the snail, *Lymnaea stagnalis*. *J. Physiol.* 351:199–216. https://doi.org/10.1113/jphysiol.1984.sp015241

Chamberlin, A., F. Qiu, S. Rebolledo, Y. Wang, S.Y. Noskov, and H.P. Larsson. 2014. Hydrophobic plug functions as a gate in voltage-gated proton channels. *Proc. Natl. Acad. Sci. USA.* 111:E273–E282. https://doi.org/10.1073/pnas.1318018111

Chamberlin, A., F. Qiu, Y. Wang, S.Y. Noskov, and H.P. Larsson. 2015. Mapping the gating and permeation pathways in the voltage-gated proton channel Hv1. *J. Mol. Biol.* 427:131–145. https://doi.org/10.1016/j.jmb.2014.11.018

Chaves, G., S. Bungert-Plümke, A. Franzen, I. Mahorivska, and B. Musset. 2020. Zinc modulation of proton currents in a new voltage-gated proton channel suggests a mechanism of inhibition. *FEBS J.* febs.15291. https://doi.org/10.1111/febs.15291

Cherny, V.V., and T.E. DeCoursey. 1999. pH-dependent inhibition of voltage-gated H^+ currents in rat alveolar epithelial cells by Zn^{2+} and other divalent cations. *J. Gen. Physiol.* 114:819–838. https://doi.org/10.1085/jgp.114.6.819

Cherny, V.V., V.S. Markin, and T.E. DeCoursey. 1995. The voltage-activated hydrogen ion conductance in rat alveolar epithelial cells is determined by the pH gradient. *J. Gen. Physiol.* 105:861–896. https://doi.org/10.1085/jgp.105.6.861

Cherny, V.V., D. Morgan, B. Musset, G. Chaves, S.M.E. Smith, and T.E. DeCoursey. 2015. Tryptophan 207 is crucial to the unique properties of the human voltage-gated proton channel, hH_V1. *J. Gen. Physiol.* 146:343–356. https://doi.org/10.1085/jgp.201511456

DeCoursey, T.E. 2003. Voltage-gated proton channels and other proton transfer pathways. *Physiol. Rev.* 83:475–579. https://doi.org/10.1152/physrev.00028.2002

DeCoursey, T.E. 2013. Voltage-gated proton channels: molecular biology, physiology, and pathophysiology of the H_V family. *Physiol. Rev.* 93:599–652. https://doi.org/10.1152/physrev.00011.2012

DeCoursey, Thomas E. 2015a. Structural revelations of the human proton channel. *Proc. Natl. Acad. Sci. USA.* 112:13430–13431. https://doi.org/10.1073/pnas.1518486112

DeCoursey, T.E. 2018. Voltage and pH sensing by the voltage-gated proton channel, H_V1. *J. R. Soc. Interface.* 15. 20180108. https://doi.org/10.1098/rsif.2018.0108

DeCoursey, Thomas E. 2015b. The Voltage-Gated Proton Channel: A Riddle, Wrapped in a Mystery, inside an Enigma. *Biochemistry.* 54:3250–3268. https://doi.org/10.1021/acs.biochem.5b00353

DeCoursey, T.E., and V.V. Cherny. 1996. Effects of buffer concentration on voltage-gated H^+ currents: does diffusion limit the conductance? *Biophys. J.* 71:182–193. https://doi.org/10.1016/S0006-3495(96)79215-9

DeCoursey, T.E., and V.V. Cherny. 1997. Deuterium isotope effects on permeation and gating of proton channels in rat alveolar epithelium. *J. Gen. Physiol.* 109:415–434. https://doi.org/10.1085/jgp.109.4.415

DeCoursey, T.E., D. Morgan, B. Musset, and V.V. Cherny. 2016. Insights into the structure and function of H_V1 from a meta-analysis of mutation studies. *J. Gen. Physiol.* 148:97–118. https://doi.org/10.1085/jgp.201611619

Eder, C., H.G. Fischer, U. Hadding, and U. Heinemann. 1995. Properties of voltage-gated currents of microglia developed using macrophage colony-stimulating factor. *Pflügers Arch.* 430:526–533. https://doi.org/10.1007/BF00373889

Fujiwara, Y., T. Kurokawa, K. Takeshita, M. Kobayashi, Y. Okochi, A. Nakagawa, and Y. Okamura. 2012. The cytoplasmic coiled-coil mediates cooperative gating temperature sensitivity in the voltage-gated H^+ channel Hv1. *Nat. Commun.* 3:816. https://doi.org/10.1038/ncomms1823

Fujiwara, Y., T. Kurokawa, K. Takeshita, A. Nakagawa, H.P. Larsson, and Y. Okamura. 2013. Gating of the designed trimeric/tetrameric voltage-gated H^+ channel. *J. Physiol.* 591:627–640. https://doi.org/10.1113/jphysiol.2012.243006

Fujiwara, Y., T. Kurokawa, and Y. Okamura. 2014. Long α helices projecting from the membrane as the dimer interface in the voltage-gated H^+ channel. *J. Gen. Physiol.* 143:377–386. https://doi.org/10.1085/jgp.201311082

Gianti, E., L. Delemotte, M.L. Klein, and V. Carnevale. 2016. On the role of water density fluctuations in the inhibition of a proton channel. *Proc. Natl. Acad. Sci. USA*. 113:E8359–E8368. https://doi.org/10.1073/pnas.1609964114

Gonzalez, C., H.P. Koch, B.M. Drum, and H.P. Larsson. 2010. Strong cooperativity between subunits in voltage-gated proton channels. *Nat. Struct. Mol. Biol*. 17:51–56. https://doi.org/10.1038/nsmb.1739

Gonzalez, C., S. Rebolledo, M.E. Perez, and H.P. Larsson. 2013. Molecular mechanism of voltage sensing in voltage-gated proton channels. *J. Gen. Physiol*. 141:275–285. https://doi.org/10.1085/jgp.201210857

Gurd, F.R., and P.E. Wilcox. 1956. Complex formation between metallic cations and proteins, peptides and amino acids. *Adv. Protein Chem*. 11: 311–427. https://doi.org/10.1016/S0065-3233(08)60424-6

Jardin, C., G. Chaves, and B. Musset. 2020. Assessing structural determinants of Zn^{2+} binding to human H_V1 via multiple MD simulations. *Biophys. J*. 118:1221–1233. https://doi.org/10.1016/j.bpj.2019.12.035

Kapus, A., R. Romanek, A.Y. Qu, O.D. Rotstein, and S. Grinstein. 1993. A pH-sensitive and voltage-dependent proton conductance in the plasma membrane of macrophages. *J. Gen. Physiol*. 102:729–760. https://doi.org/10.1085/jgp.102.4.729

Kariev, A.M., and M.E. Green. 2018. The role of proton transport in gating current in a voltage gated ion channel, as shown by quantum calculations. *Sensors (Basel)*. 18:3143. https://doi.org/10.3390/s18093143

Koch, H.P., T. Kurokawa, Y. Okochi, M. Sasaki, Y. Okamura, and H.P. Larsson. 2008. Multimeric nature of voltage-gated proton channels. *Proc. Natl. Acad. Sci. USA*. 105:9111–9116. https://doi.org/10.1073/pnas.0801553105

Krężel, A., and W. Maret. 2016. The biological inorganic chemistry of zinc ions. *Arch. Biochem. Biophys*. 611:3–19. https://doi.org/10.1016/j.abb.2016.04.010

Kulleperuma, K., S.M.E. Smith, D. Morgan, B. Musset, J. Holyoake, N. Chakrabarti, V.V. Cherny, T.E. DeCoursey, and R. Pomès. 2013. Construction and validation of a homology model of the human voltage-gated proton channel hH_V1. *J. Gen. Physiol*. 141:445–465. https://doi.org/10.1085/jgp.201210856

Lee, C.H., and R. MacKinnon. 2019. Voltage sensor movements during hyperpolarization in the HCN channel. *Cell*. 179:1582–1589.e7. https://doi.org/10.1016/j.cell.2019.11.006

Lee, S.Y., J.A. Letts, and R. Mackinnon. 2008. Dimeric subunit stoichiometry of the human voltage-dependent proton channel Hv1. *Proc. Natl. Acad. Sci. USA*. 105:7692–7695. https://doi.org/10.1073/pnas.0803277105

Li, Q., S. Wanderling, M. Paduch, D. Medovoy, A. Singharoy, R. McGreevy, C.A. Villalba-Galea, R.E. Hulse, B. Roux, K. Schulten, et al. 2014. Structural mechanism of voltage-dependent gating in an isolated voltage-sensing domain. *Nat. Struct. Mol. Biol*. 21:244–252. https://doi.org/10.1038/nsmb.2768

Li, Q., R. Shen, J.S. Treger, S.S. Wanderling, W. Milewski, K. Siwowska, F. Bezanilla, and E. Perozo. 2015. Resting state of the human proton channel dimer in a lipid bilayer. *Proc. Natl. Acad. Sci. USA*. 112: E5926–E5935. https://doi.org/10.1073/pnas.1515043112

Lishko, P.V., I.L. Botchkina, A. Fedorenko, and Y. Kirichok. 2010. Acid extrusion from human spermatozoa is mediated by flagellar voltage-gated proton channel. *Cell*. 140:327–337. https://doi.org/10.1016/j.cell.2009.12.053

Mahaut-Smith, M.P. 1989a. The effect of zinc on calcium and hydrogen ion currents in intact snail neurones. *J. Exp. Biol*. 145:455–464.

Mahaut-Smith, M.P. 1989b. Separation of hydrogen ion currents in intact molluscan neurones. *J. Exp. Biol*. 145:439–454.

Mony, L., T.K. Berger, and E.Y. Isacoff. 2015. A specialized molecular motion opens the Hv1 voltage-gated proton channel. *Nat. Struct. Mol. Biol*. 22: 283–290. https://doi.org/10.1038/nsmb.2978

Morgan, D., B. Musset, K. Kulleperuma, S.M.E. Smith, S. Rajan, V.V. Cherny, R. Pomès, and T.E. DeCoursey. 2013. Peregrination of the selectivity filter delineates the pore of the human voltage-gated proton channel hH_V1. *J. Gen. Physiol*. 142:625–640. https://doi.org/10.1085/jgp.201311045

Musset, B., V.V. Cherny, D. Morgan, Y. Okamura, I.S. Ramsey, D.E. Clapham, and T.E. DeCoursey. 2008. Detailed comparison of expressed and native voltage-gated proton channel currents. *J. Physiol*. 586:2477–2486. https://doi.org/10.1113/jphysiol.2007.149427

Musset, B., S.M.E. Smith, S. Rajan, V.V. Cherny, D. Morgan, and T.E. DeCoursey. 2010a. Oligomerization of the voltage-gated proton channel. *Channels (Austin)*. 4:260–265. https://doi.org/10.4161/chan.4.4.12789

Musset, B., S.M.E. Smith, S. Rajan, V.V. Cherny, S. Sujai, D. Morgan, and T.E. DeCoursey. 2010b. Zinc inhibition of monomeric and dimeric proton channels suggests cooperative gating. *J. Physiol*. 588:1435–1449. https://doi.org/10.1113/jphysiol.2010.188318

Musset, B., S.M.E. Smith, S. Rajan, D. Morgan, V.V. Cherny, and T.E. DeCoursey. 2011. Aspartate 112 is the selectivity filter of the human voltage-gated proton channel. *Nature*. 480:273–277. https://doi.org/10.1038/nature10557

Paoletti, P., P. Ascher, and J. Neyton. 1997. High-affinity zinc inhibition of NMDA NR1-NR2A receptors. *J. Neurosci*. 17:5711–5725. https://doi.org/10.1523/JNEUROSCI.17-15-05711.1997

Pettersen, E.F., T.D. Goddard, C.C. Huang, G.S. Couch, D.M. Greenblatt, E.C. Meng, and T.E. Ferrin. 2004. UCSF Chimera--a visualization system for exploratory research and analysis. *J. Comput. Chem*. 25:1605–1612. https://doi.org/10.1002/jcc.20084

Pupo, A., D. Baez-Nieto, A. Martínez, R. Latorre, and C. González. 2014. Proton channel models filling the gap between experimental data and the structural rationale. *Channels (Austin)*. 8:180–192. https://doi.org/10.4161/chan.28665

Qiu, F., A. Chamberlin, B.M. Watkins, A. Ionescu, M.E. Perez, R. Barro-Soria, C. González, S.Y. Noskov, and H.P. Larsson. 2016. Molecular mechanism of Zn^{2+} inhibition of a voltage-gated proton channel. *Proc. Natl. Acad. Sci. USA*. 113:E5962–E5971. https://doi.org/10.1073/pnas.1604082113

Ramsey, I.S., M.M. Moran, J.A. Chong, and D.E. Clapham. 2006. A voltage-gated proton-selective channel lacking the pore domain. *Nature*. 440: 1213–1216. https://doi.org/10.1038/nature04700

Ramsey, I.S., Y. Mokrab, I. Carvacho, Z.A. Sands, M.S.P. Sansom, and D.E. Clapham. 2010. An aqueous H^+ permeation pathway in the voltage-gated proton channel Hv1. *Nat. Struct. Mol. Biol*. 17:869–875. https://doi.org/10.1038/nsmb.1826

Randolph, A.L., Y. Mokrab, A.L. Bennett, M.S. Sansom, and I.S. Ramsey. 2016. Proton currents constrain structural models of voltage sensor activation. *eLife*. 5. e18017. https://doi.org/10.7554/eLife.18017

Schrenzel, J., D.P. Lew, and K.H. Krause. 1996. Proton currents in human eosinophils. *Am. J. Physiol*. 271:C1861–C1871. https://doi.org/10.1152/ajpcell.1996.271.6.C1861

Takeshita, K., S. Sakata, E. Yamashita, Y. Fujiwara, A. Kawanabe, T. Kurokawa, Y. Okochi, M. Matsuda, H. Narita, Y. Okamura, et al. 2014. X-ray crystal structure of voltage-gated proton channel. *Nat. Struct. Mol. Biol*. 21:352–357. https://doi.org/10.1038/nsmb.2783

Thomas, R.C., and R.W. Meech. 1982. Hydrogen ion currents and intracellular pH in depolarized voltage-clamped snail neurones. *Nature*. 299: 826–828. https://doi.org/10.1038/299826a0

Thomas, S., V.V. Cherny, D. Morgan, L.R. Artinian, V. Rehder, S.M.E. Smith, and T.E. DeCoursey. 2018. Exotic properties of a voltage-gated proton channel from the snail *Helisoma trivolvis*. *J. Gen. Physiol*. 150:835–850. https://doi.org/10.1085/jgp.201711967

Tombola, F., M.H. Ulbrich, and E.Y. Isacoff. 2008. The voltage-gated proton channel Hv1 has two pores, each controlled by one voltage sensor. *Neuron*. 58:546–556. https://doi.org/10.1016/j.neuron.2008.03.026

Tombola, F., M.H. Ulbrich, S.C. Kohout, and E.Y. Isacoff. 2010. The opening of the two pores of the Hv1 voltage-gated proton channel is tuned by cooperativity. *Nat. Struct. Mol. Biol*. 17:44–50. https://doi.org/10.1038/nsmb.1738

van Keulen, S.C., E. Gianti, V. Carnevale, M.L. Klein, U. Rothlisberger, and L. Delemotte. 2017. Does proton conduction in the voltage-gated H^+ channel hHv1 involve Grotthuss-like hopping via acidic residues? *J. Phys. Chem. B*. 121:3340–3351. https://doi.org/10.1021/acs.jpcb.6b08339

Webster, S.M., D. Del Camino, J.P. Dekker, and G. Yellen. 2004. Intracellular gate opening in Shaker K^+ channels defined by high-affinity metal bridges. *Nature*. 428:864–868. https://doi.org/10.1038/nature02468

Wood, M.L., E.V. Schow, J.A. Freites, S.H. White, F. Tombola, and D.J. Tobias. 2012. Water wires in atomistic models of the Hv1 proton channel. *Biochim. Biophys. Acta*. 1818:286–293. https://doi.org/10.1016/j.bbamem.2011.07.045